Review

Samoil Sekulovski and Simon Trowitzsch*

# Transfer RNA processing – from a structural and disease perspective

https://doi.org/10.1515/hsz-2021-0406
Received November 2, 2021; accepted May 24, 2022;
published online June 21, 2022

**Abstract:** Transfer RNAs (tRNAs) are highly structured non-coding RNAs which play key roles in translation and cellular homeostasis. tRNAs are initially transcribed as precursor molecules and mature by tightly controlled, multistep processes that involve the removal of flanking and intervening sequences, over 100 base modifications, addition of non-templated nucleotides and aminoacylation. These molecular events are intertwined with the nucleocytoplasmic shuttling of tRNAs to make them available at translating ribosomes. Defects in tRNA processing are linked to the development of neurodegenerative disorders. Here, we summarize structural aspects of tRNA processing steps with a special emphasis on intron-containing tRNA splicing involving tRNA splicing endonuclease and ligase. Their role in neurological pathologies will be discussed. Identification of novel RNA substrates of the tRNA splicing machinery has uncovered functions unrelated to tRNA processing. Future structural and biochemical studies will unravel their mechanistic underpinnings and deepen our understanding of neurological diseases.

**Keywords:** end maturation; endonuclease; neurodegenerative disorders; RNA processing; structural biology; tRNA splicing.

## Introduction

All organisms of the three domains of life ubiquitously produce and utilize tRNAs. Their central role as supplier of amino acids for protein synthesis is well-established. By numbers, tRNAs are the most abundant RNA species in cells with approximately 3–10 $\times$ $10^7$ molecules per cell, whereas they are second behind ribosomal RNAs considering their total mass (Palazzo and Lee 2015). Mature tRNAs can vary greatly in sequence length, ranging from 76 to 93 nucleotides, and comprise a multitude of base modifications: some almost universal and others specific for a subspecies of tRNAs. These modifications tremendously diversify the tRNA pool (Schimmel 2018). Due to the constantly increasing number of more than 100 enzymatic pathways, we do not discuss tRNA modifying enzymes but recommend the following excellent reviews (Han and Phizicky 2018; Krutyholowa et al. 2019; Suzuki 2021).

Although the first high-resolution tRNA structure was already solved in 1973 (Kim et al. 1973), protein structures of the tRNA processing pathway have been solved much later and are still being investigated. In eukaryotes, tRNAs are transcribed by RNA polymerase III as precursor molecules (pre-tRNAs) with a subset of about 6% of all tRNAs carrying introns (Chan and Lowe 2016). For their maturation, pre-tRNAs undergo several processing steps and modifications. Typically, the canonical cascade of processing is described as removal of 5′ leader and 3′ trailer sequences by RNase P and RNase Z, respectively, addition of the terminal CCA trinucleotide by ATP(CTP):tRNA nucleotidyltransferase, nuclear export by exportin-t and splicing of intron-containing tRNAs by tRNA splicing endonuclease (TSEN) and tRNA ligase. Interestingly, the order of events does not seem to be as strict as described here. For example, there is contradicting evidence that removal of 5′ trailer sequences does not necessarily precede cleavage of the 3′ extension and even occurs in a reverse order for some tRNA species (O'Connor and Peebles 1991; Kufel and Tollervey 2003; Maraia and Lamichhane 2011). An even broader ambiguity is observed for tRNA modifying enzymes concerning their spatio-temporal organization of activity (Chatterjee et al. 2018; Kramer and Hopper 2013; Nostramo and Hopper 2020). Here, we focus on several nuclear and cytosolic processing steps of pre-tRNAs, discussing structural aspects of tRNA recognition,

***Corresponding author: Simon Trowitzsch**, Institute of Biochemistry, Biocenter, Goethe University Frankfurt, Max-von-Laue-Strasse 9, D-60438 Frankfurt/Main, Germany, E-mail: trowitzsch@biochem.uni-frankfurt.de. https://orcid.org/0000-0001-9143-766X
**Samoil Sekulovski,** Institute of Biochemistry, Biocenter, Goethe University Frankfurt, Max-von-Laue-Strasse 9, D-60438 Frankfurt/Main, Germany. https://orcid.org/0000-0002-6732-9236

binding, and catalysis during end maturation, nuclear export, and splicing. When appropriate we refer the reader to detailed reviews for in-depth information.

## Structure of transfer RNAs

The overall three-dimensional fold of tRNA precursors is key for their interaction with modifying enzymes. Despite their diversity, tRNAs universally adopt their characteristic L-shaped structure (Figure 1). The complicated folding process can be comprehended by looking at the underlying secondary structures. Formed by designated base pairs, four stem-loop structures constitute the tRNA cloverleaf (Figure 1A). Starting at the 5′ terminus, the tRNA consists of the acceptor stem, the D-arm, the anticodon arm, a variable loop, and the TΨC arm. The acceptor stem unites the 5′ terminus and single-stranded 3′ terminus consisting of discriminator base and a CCA triplet, key residues for aminoacylation. Owing its name to the conserved dihydrouridine base (D), the D arm forms the L-fold of tRNAs together with the TΨC arm. The anticodon stem carries the anticodon loop for base pairing with mRNA codons and translation specificity. The variable arm mainly contributes to the length variety of mature tRNAs which span from 76 to 93 nucleotides. Therefore, the standard numbering of tRNA residues omits variable nucleotides and always ends with the CCA triplet as nucleotides 74 to 76. Lastly, the TΨC-arm, named after the conserved bases thymidine (T), pseudouridine (Ψ), and cytidine (C), facilitates interactions with the ribosome. To form the L-shaped structure, the 5 bp TΨC-stem stacks coaxially onto the 7 bp acceptor stem resulting in the 12 bp minihelix on top of the tRNA (Figure 1B). D-stem and anticodon stem similarly stack onto each other to form a 9 to 10 bp stem helix which merges into the anticodon loop. These two helices connect perpendicularly by tertiary base pairing and stacking between the D- and TΨC-loop at the so-called elbow, forming the L-fold (Figure 1C). An intricate network of interactions stabilizes the L-shape. A $G^{19}$:$C^{56}$ Watson–Crick base pair defines the outermost part of the elbow where one side is facing the solvent. Additionally, $G^{18}$ and the conserved $\Psi^{55}$ form a single hydrogen bond while $G^{18}$ also intercalates between nucleotides 57 and 58. Consequently, the bases $G^{19}$, $C^{56}$, $G^{57}$, $G^{18}$, $\Psi^{55}$, and $A^{58}$ perform continuous stacking interactions intertwining the D- and TΨC-loop. Noteworthy, the identity of the mentioned nucleotides is not absolute for every tRNA, but we refer to the most common for the sake of simplicity. The solvent exposed $G^{19}$:$C^{56}$ base pair is a hot spot of tRNA binding for numerous proteins and RNAs as we will also emphasize in this review. A likely explanation for attractiveness of this base pair is the ease of probing the mature tRNA fold, a key requirement for the fidelity of several processing steps, nuclear export, and aminoacylation (Rich and RajBhandary 1976; Zhang and Ferre-D'Amare 2016).

### 5′ end processing of transfer RNAs

Cleavage of the tRNA 5′ leader sequence is a universally performed task of the ancient endoribonuclease complex

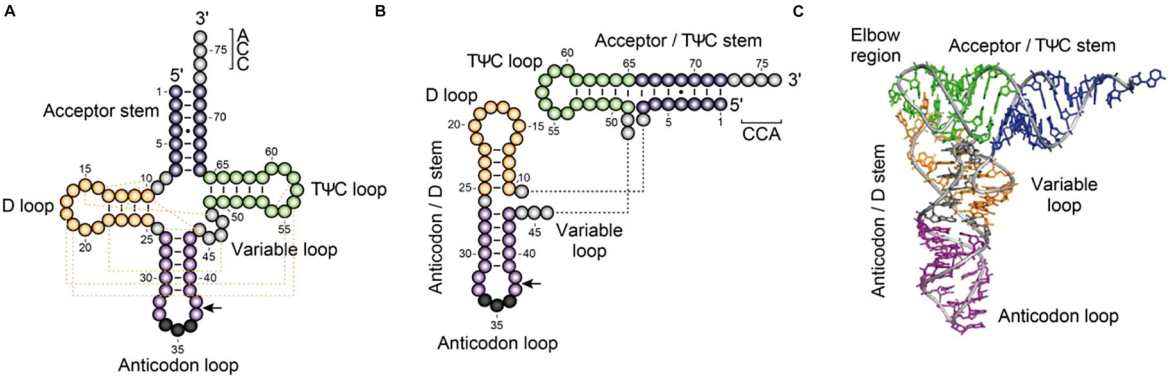


**Figure 1:** Structure of transfer RNAs.
(A) Cloverleaf structure showing secondary (black lines) and tertiary (orange dashed lines) interactions. The tRNA is subdivided into acceptor stem, D arm, anticodon arm, variable loop and TΨC arm. The $G^{19}$:$C^{56}$ and $G^{18}$:$\Psi^{55}$ base pairs bridge the D-loop and TΨC loop to form the L-shaped tRNA fold. Further tertiary interactions between D arm and variable loop stabilize the 3D structure. (B) Intermediate fold. TΨC stem and acceptor stem as well as D stem and anticodon stem coaxially stack onto each other forming a 12 bp and 9–10 bp helix, respectively. (C) Three-dimensional (3D) structure of yeast $tRNA^{Phe}$ (PDB ID 1EHZ). Base pairing and stacking interactions from (A) and (B) form the characteristic L-shape of tRNA. The main tRNA interaction sites for proteins and other RNAs are exposed at the three outermost positions: CCA triplet, elbow region, and anticodon triplet.

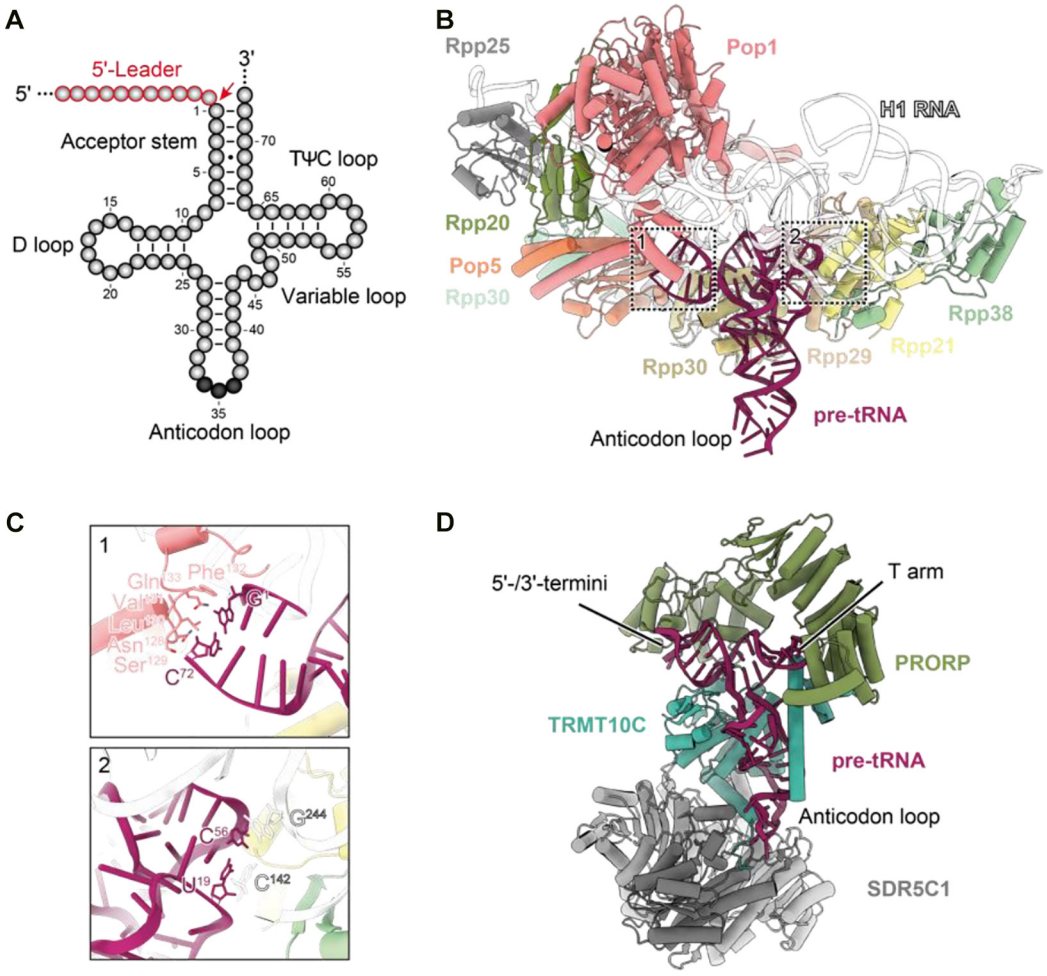


**Figure 2:** Recognition of precursor tRNA by 5′ processing RNase P.
(A) RNase P produces the mature 5′ terminus by endonucleolytic cleavage of the pre-tRNA 5′ leader. (B) Overview of human RNase P-tRNA complex. RNase P protein subunits build a right-hand-like structure to wrap around the catalytic H1 RNA and the tRNA substrate. The tRNA TΨC/acceptor minihelix is bound by a double anchor mechanism via interactions of H1 RNA with the elbow region and Pop1 with the termini. Only the conserved length of 12 bp allows the minihelix to bind between the anchors. An interface of Rpp29 and Rpp30 binds the D/anticodon stem. (C) Zoom-in on termini (1) and elbow (2). A loop of Pop1 mainly interacts with the terminal $G^1$:$C^{72}$ base pair by hydrophobic residues. $Asn^{128}$ and $Gln^{133}$ are proximal to $C^{72}$ and $G^1$ for a potential stacking interaction, respectively. The $U^{19}$:$C^{56}$ base pair in the elbow region stacks onto the H1 nucleobases $C^{142}$ and $G^{244}$ (PDB ID 6AHU). (D) Overview of human mitochondrial (mt) RNase P–tRNA complex. Similar to the RNase P ribozyme, mtRNase P wraps around the acceptor stem using the PRORP subunit. Additionally, the TRMT10C-SDR5C1 subcomplex binds the anticodon arm including a specific interaction with nucleotide 33 and putatively senses or stabilizes the distorted tRNA conformation (PDB ID 7ONU).

RNase P (Ellis and Brown 2009) (Figure 2). Alongside the ribosome, RNase P arose before divergence of the last universal common ancestor into today's three domains of life (Gray and Gopalan 2020). The key component of RNase P is the catalytic RNA (Ellis and Brown 2009; Guerrier-Takada et al. 1983). However, comparison between Bacteria, Archaea, and Eukarya, revealed a structural and functional substitution of parts of the RNA by proteins with increasing complexity of the organism (Esakova and Krasilnikov 2010). Noteworthy, protein-only forms of RNase P were identified in mitochondria of metazoans and extensively characterized (Figure 2D) (Bhatta et al. 2021; Holzmann et al. 2008; Lechner et al. 2015). Additional functions of RNase P were widely reported, including processing of the 4.5S RNA of the signal recognition particle, transfer-messenger (tm) RNA in *Escherichia coli*, and maturation of small nucleolar RNAs in yeast (Coughlin et al. 2008; Guerrier-Takada and Altman 1984; Komine et al. 1994). In this review, we mainly describe human nuclear RNase P and recommend these reviews for further reading (Ellis and Brown 2009; Esakova and Krasilnikov 2010; Gray and Gopalan 2020; Schencking et al. 2020).

Human RNase P is a large RNP consisting of 10 protein subunits and one catalytic RNA (Wu et al. 2018) (Figure 2B).

The RNA component (H1 RNA) contains a catalytic (C) and specificity (S) domain, which form a helical core with long-range RNA–RNA interactions maintaining the tertiary structure. Main interactions with the substrate are driven by five universally conserved regions, CR-I to CR-V, which cluster into two structural modules. CR-I/CR-IV/CR-V is the key component for catalysis whereas CR-II/CR-III mediates substrate recognition. Human RNase P adopts an elongated conformation by a network of protein–protein and protein–RNA interactions. The protein subunits are connected in a chain-like fashion to form a right-hand-shaped clamp with finger, palm and wrist modules. The protein clamp wraps around the H1 RNA and buries a large surface area of 13,960 Å$^2$. The catalytic C domain of the RNA binds between the palm and finger modules while the S domain packs against the wrist. The H1 RNA thereby acts as a scaffold which interacts with all protein subunits allowing to organize and stabilize the extended conformation of the whole complex (Figure 2B).

In the human RNase P-tRNA complex, the acceptor stem and TΨC arm of tRNA bind in an open pocket between C domain and CR-II/CR-III module in the S domain (Figure 2B). The tRNA anticodon stem interacts with a complementary surface formed by the palm and wrist modules of the protein clamp. The elbow of the tRNA is recognized by stacking of a cytosine and guanine in the CR-II/CR-III module with the U$^{19}$:C$^{56}$ base pair, which connects the D and TΨC loop of the tRNA (Figure 2C). In proximity to the termini, a coiled loop in the protein subunit Pop1 protrudes into the tRNA acceptor stem and directly interacts with the G$^1$:C$^{72}$ base pair (Figure 2C). Hence, Pop1 aids in positioning the 5′ cleavage site of tRNA in the catalytic centre of H1 RNA. Both interaction sites do not recognize specific sequences but rather act as anchors which measure the conserved distance of 12 bp between TΨC loop and cleavage site (5 bp TΨC stem + 7 bp acceptor stem). This implies a general mechanism of binding for RNase P by utilizing conserved structural features of tRNAs which would also allow for excluding erroneously folded molecules. Interestingly, the human mtRNase P-tRNA complex revealed different interactions for substrate recognition (Figure 2D). Mitochondrial tRNA typically lacks the elbow region due to high variability in the T and D loops and therefore the PRORP subunit only interacts with the T loop backbone. Instead, subunits TRMT10C and SDR5C1 recognize key features of mitochondrial tRNAs including charge, the distorted conformation, and nucleobase 33 of the anticodon loop (Bhatta et al. 2021).

In nuclear RNase P, the 5′ leader cleavage reaction is dependent on divalent metal ions (likely $Mg^{2+}$) (Kirsebom and Trobro 2009). Unfortunately, the resolution of the human RNase P-tRNA complex does not allow identification of ions in the catalytic centre. Although the authors performed a sophisticated approach to capture the RNase P-tRNA complex under turnover conditions, the cryo-EM structure was solved in a post cleavage state missing a 5′ leader sequence (Wu et al. 2018). However, as comparative analysis of human and *Thermotoga maritima* RNase P-tRNA complexes revealed near identical configuration of the active sites, it was hypothesized that the cleavage mechanism is conserved from bacteria to humans (Reiter et al. 2010). The crystal structure of *T. maritima* RNase P features two putative catalytic magnesium ions (M1 and M2). In the derived transition state model, the M1 metal is proposed to coordinate the scissile phosphate oxygens of the tRNA. Thereby, a hydroxyl ion can perform an $S_N2$-type nucleophilic attack. Subsequently, the M2 metal stabilizes the transition state and mediates proton transfer to the 3′ scissile oxygen. In the future, it will be interesting to investigate human RNase P in complex with tRNA to verify the proposed catalytic mechanism by using catalytically inactive H1 RNA or non-cleavable tRNA.

## 3′ end processing of transfer RNAs

The 3′ trailer of most precursor tRNAs is removed by the conserved endoribonuclease RNase Z (Schiffer et al. 2002) (Figure 3A). However, 3′ trimming by exonucleases is also described for many cases (Copela et al. 2008; Ozanick et al. 2009; Wellner et al. 2018b). Different tRNA 3′ processing pathways and their biological relevance are discussed in these thorough reviews (Maraia and Lamichhane 2011; Wellner et al. 2018a). RNase Z is encoded in the genomes of most eukaryotes and archaea, and many bacteria. In eukaryotes, two forms of RNase Z can be found, a long RNase Z$^L$ and a short RNase Z$^S$, while in prokaryotes only the short form exists. It is proposed that RNase Z$^L$ arose from gene duplication events of an ancestral RNase Z$^S$ gene due to the structural similarity of the N- and C-terminal domains (Tavtigian et al. 2001). Due to the lack of eukaryotic RNase Z structures with substrate, we review the structure of the *Bacillus subtilis* homologue RNase Z$^S$ in complex with tRNA and draw conclusions for the human RNase Z$^L$ (ELAC2) (Li de la Sierra-Gallay et al. 2006).

The RNase Z$^S$ enzyme is assembled as a homodimer of its β-lactamase domains, each with a flexible tRNA binding arm. Belonging to the family of metallo-β-lactamases, RNase Z utilizes the conserved S/THxHxDH motif (where x is any amino acid) to coordinate two zinc metal ions for enzyme catalysis (Ishii et al. 2005; Li de la Sierra-Gallay

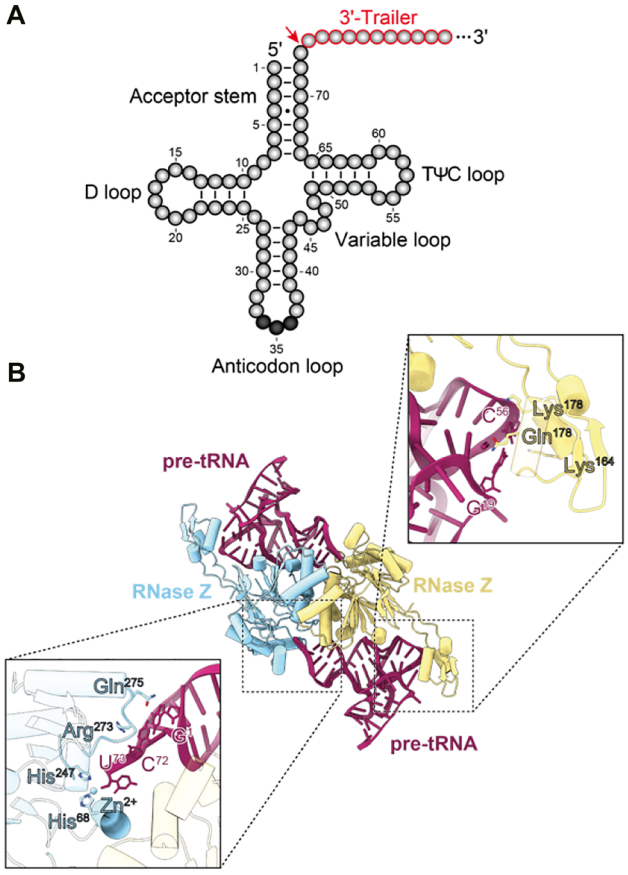


**Figure 3:** Recognition of precursor tRNA by 3′ processing RNase Z. (A) The 3′ trailer is removed by endonucleolytic cleavage via RNase Z. (B) Overview structure of the RNase Z dimer in complex with tRNA. The two tRNAs are bound symmetrically by the dimer. One of the subunits is primarily responsible for binding while the other performs the cleavage of the trailer sequence. The upper close-up panel shows the interaction between the flexible tRNA binding arm of subunit B and the tRNA elbow. The proximal lysines interact with the tRNA backbone phosphate while the $Gln^{175}$ could hydrogen bond with $G^{19}$. The lower panel features the tRNA interactions of the other subunit close to the catalytic site of subunit A. $Arg^{273}$ is proposed to sense the presence of tRNA by acting as a bridge between substrate and protein. The close-by $Gln^{275}$ is a good candidate for interaction with $G^{1}$ by stacking or hydrogen bonding. As one of the catalytic residues $His^{247}$ hydrogen bonds with the ribose of $U^{73}$ to coordinate the nucleoside in the active centre. One of the catalytic $Zn^{2+}$ ions is resolved, being coordinated by $His^{68}$ (PDB ID 2FK6).

et al. 2005; Schilling et al. 2005). As a dimer, RNase $Z^{S}$ binds two tRNAs at the same time in a symmetric manner (Figure 3B). The TΨC arm and acceptor stem of the tRNA nestle to a basic patch on the dimer surface. Noteworthy, tRNA is primarily recognized by two lysine/arginine-rich motifs on the surface of one subunit but is cleaved by the adjacent other. Reminiscent of the RNase P double anchor, the flexible arm of one subunit interacts with the $G^{19}$:$C^{56}$ base pair and the helix α7 of the other subunit with the $G^{1}$:$C^{72}$ base pair and discriminator base $U^{73}$ (Figure 3B). The protein interacts with the conserved guanosines 1 and 19 by hydrogen bonding which underpins the importance of mature tRNA fold for recognition. As the complex was captured in a post-processing state, there is no density for the 3′ trailer. However, the narrowing of the protein channel at the termini implies that only a single-stranded 3′ extension can protrude into the active centre. This arrangement possibly explains why tRNAs with long 5′ extensions are poor substrates for RNase Z processing (Pellegrini et al. 2003).

To describe the interaction between human ELAC2 and tRNA, the Condon lab modelled the predicted structure of ELAC2 on the bacterial dimer (Redko et al. 2007). Although the N-terminal domain of ELAC2 seems to contain a flexible arm for tRNA interaction, it lacks key histidine residues for zinc-coordination at the catalytic site. Contrastingly, the C-terminal domain has a complete active site but instead lacks a tRNA binding arm. Therefore, this model proposes that eukaryotic RNase $Z^{L}$ only binds one tRNA for processing which agrees with previous predictions (Redko et al. 2007).

Since the *B. subtilis* structure of RNase Z shows a post-processing state, the catalysis mechanism was derived from a crystal structure of human glyoxolase II which also belongs to the metallo-β-lactamases and has a virtually identical active site (Cameron et al. 1999a,b). The two $Zn^{2+}$ ions are coordinated by five histidines, two aspartates, a water molecule, and a phosphate group (Li de la Sierra-Gallay et al. 2005). By deprotonation of a water molecule by an aspartate, the resulting hydroxide performs a nucleophilic attack on the phosphate between nucleotide 73 and 74, which is polarized by the two $Zn^{2+}$ ions. After cleavage of the phosphodiester, the 3′ oxygen of the discriminator nucleotide receives a proton from another water molecule for stabilization. Hence, the tRNA is processed to its mature 3′ terminus and fit for addition of the CCA triplet. Due to the lack of structures for eukaryotic RNase Z enzymes, future studies will clarify if the same structural features and mechanism exist.

## CCA addition

A ubiquitously conserved characteristic of tRNAs from all three domains of life is the 3′ terminal CCA sequence (Figure 4A). This sequence is fundamental for charging of tRNAs with their respective amino acids (Sprinzl and Cramer 1979; Tamura and Hasegawa 1997). Furthermore, the CCA triplet has been shown to aid the positioning of its attached amino acid in the ribosomal A-site and the

catalysis of peptide bond formation (Green and Noller 1997; Kim and Green 1999; Liu et al. 1998; Nissen et al. 2000; Weinger et al. 2004; Wellner et al. 2018a). Consequently, the 3′-CCA end is a key recognition motif for nuclear tRNA export and cells thoroughly monitor the integrity of tRNA 3′ termini (Arts et al. 1998; Kutay et al. 1998; Lipowsky et al. 1999). The addition of CCA is catalysed by a template-independent RNA polymerase, ATP(CTP):tRNA nucleotidyltransferase, CCA-adding enzyme or CCase. Besides their transferase function, CCases have been shown to repair and maintain the 3′-CCA ends but can also tag erroneous tRNAs for degradation by addition of a second CCA triplet (Wellner et al. 2018a; Wilusz et al. 2011). Here we focus on the structural aspects of the CCA addition and refer to these thorough reviews on CCase in tRNA quality control (Lizano et al. 2008; Wellner et al. 2018a).

CCA-adding enzymes are classified into archaeal class I and eubacterial and eukaryotic class II families. Noteworthy, some eubacteria like *Aquifex aeolicus* synthesize the 3′-CCA end by utilizing two distinct but closely related CC-adding and A-adding enzymes in concert. Although a crystal structure for human CCase is available, it was not solved in complex with a tRNA (Augustin et al. 2003). Due to the availability of the CC-adding class II enzyme from *A. aeolicus* in complex with immature tRNA, binding of and CCA synthesis to tRNA will be discussed based on the results of the eubacterial enzyme (Yamashita et al. 2014).

The enzyme adopts a seahorse-like structure which is accordingly subdivided into a head, neck, body, and tail domain from the N- to the C-terminus (Figure 4B). The helix α23 stacks onto the $G^{19}$:$C^{56}$ base pair whereas the body and neck domains of the protein bind the acceptor stem. Head and neck domain form a cleft to encase the 3′ part of the tRNA. Nucleotides $G^{70}$, $C^{72}$ and $A^{73}$ form a hydrogen bond network with a glutamate and two arginine residues in proximity. The 5′ terminus of the tRNA is bound by a loop between helices α17 and α18 by hydrogen bonding between the phosphate backbone and main chain NH groups of the polypeptide. The terminal $G^{1}$:$C^{72}$ base pair stacks onto two phenylalanines of the β4 sheet in the head domain. The 3′ terminal discriminator base $A^{73}$ is oriented within the active site and gets only stabilized by stacking interactions with an incoming CTP.

As sequential structures of class II CCA-adding enzyme in complex with tRNA are so far missing for the individual nucleotide addition steps, the mechanism remains partly elusive. However, the crystal structures of CC-adding enzyme from *A. aeolicus* with tRNA resolved most parts of the two cytosine addition steps (Yamashita et al. 2014). As this goes beyond the scope of this review, we will summarize only the most important aspects of the mechanism. Please refer to this review for in detail reading (Tomita and Yamashita 2014). For the addition of the first C, the discriminator nucleoside enters the active site. The incoming CTP and $A^{73}$ interact via base stacking whereas

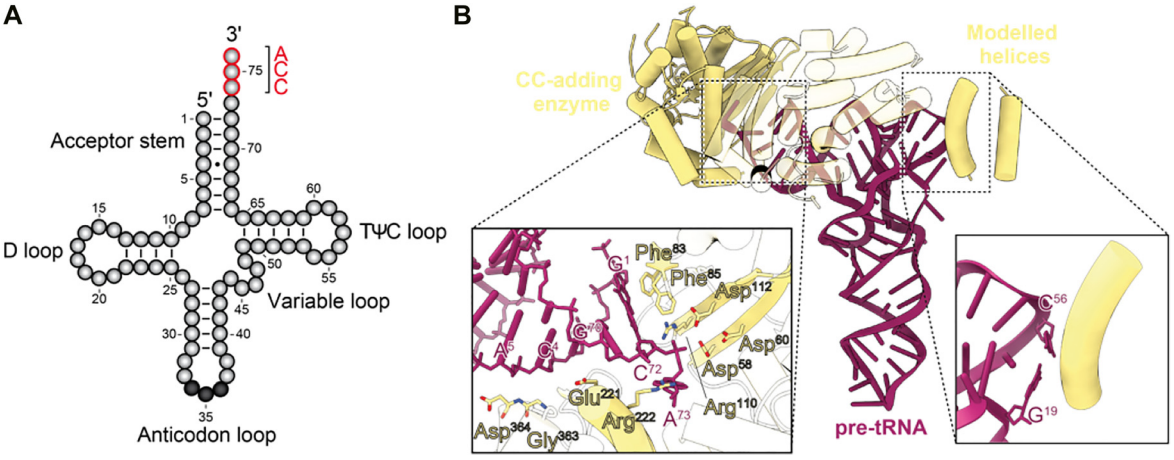


**Figure 4:** Structure of CC-adding enzyme in complex with tRNA.
(A) For maturation, a CCA triplet is added at the tRNA 3′ terminus in a one-step or two-step reaction. (B) Overview of tRNA binding by CC-adding enzyme. Main interactions focus on the tRNA termini and elbow region. In the left panel, the extensive interaction network between the 5′ and 3′ termini and the protein is shown in detail. The peptide backbone of $Asp^{364}$ and $Gly^{363}$ hydrogen bonds with the phosphate backbone of $A^{5}$ and $C^{4}$, respectively. $Glu^{221}$ and $Arg^{222}$ form hydrogen bonds with the $G^{70}$ ribose and $C^{72}$ phosphate, each. The $G^{1}$:$C^{72}$ base pair stacks onto $Phe^{83}$ and $Phe^{85}$. While the phosphate of $A^{73}$ forms a hydrogen bond with $Arg^{110}$, the nucleobase remains rather flexible until a CTP binds in the active pocket. The three catalytic aspartates $Asp^{58}$, $Asp^{60}$, and $Asp^{112}$, are centred around this phosphate for nucleotide addition. The C-terminal tail helix of the CC-adding enzyme stacks onto the $G^{19}$:$C^{56}$ base pair in a not fully resolved manner (PDB ID 3WFQ).

the CTP triphosphate and A73 ribose 3′–OH group are close to three catalytic aspartates and a $Mg^{2+}$. Another putative magnesium ion would be coordinated to one of the catalytic aspartates, and could act as a general base to activate the tRNA 3′ OH for the nucleotidyltransfer reaction. Hence, a nucleophilic attack from the 3′ OH to the α-phosphate of the incoming CTP would transfer the nucleotide while pyrophosphate is released. This pyrophosphate release triggers the translocation of the tRNA which rotates by approximately 25°. Controversially, the authors later published a structure of *T. maritima* CCA-adding enzyme with CCA-containing tRNA, rather suggesting a rearrangement of the 3′ end and active pocket than rotation and translocation of the tRNA (Yamashita and Tomita 2016). Notwithstanding, the newly added $C^{74}$ is placed in the active centre of the enzyme and the second cytosine addition proceeds by the same mechanism. Although it is thought that the CCA addition is catalysed by a similar mechanism, high resolution structures of class II CCA-adding enzymes in complex with tRNAs at different addition steps will be needed to elucidate the complete process. In this perspective, the *T. maritima* structure of CCA-adding enzyme in complex with CCA-containing tRNA already revealed a release or 3′ mature tRNA recognition state after the transferase reaction (Yamashita and Tomita 2016). Here, the tRNA is only rotated into the release state after CCA addition while mature CCA-tRNA would accordingly bind in this tilted state, preventing the 3′ end from entering the catalytic site. The ambiguities between the rotation and translocation model for *A. aeolicus* CC-adding enzyme and the rigid model for *T. maritima* CCA-adding enzyme underpin the necessity for further experiments.

## Nuclear export of transfer RNAs

tRNAs need to be transported across the nuclear envelope in an energy consuming fashion to fulfil their role as key molecules during protein synthesis. This translocation is mainly mediated by a nucleo-cytoplasmic transport factor of the karyopherin-β family, exportin-t (Chatterjee et al. 2018; Hopper and Nostramo 2019). Interestingly, other transport factors have also been implicated in nuclear (re-) export of tRNA (Calado et al. 2002; Wu et al. 2015).

Exportin-t driven tRNA export is regulated by the small GTPase Ran. The GTP-bound form of Ran (RanGTP) resides predominantly in the nucleus, while the GDP-bound form is found in the cytosol. Only in the presence of RanGTP, exportin-t binds mature tRNA. The ternary tRNA-exportin-t-RanGTP complex translocates through the nuclear pore complex (NPC) and disassembles in the cytosol by hydrolysis of Ran-bound GTP. A crystal structure of the exportin-t homologue Xpot from *Schizosaccharomyces pombe* was solved in complex with minimal binding portions of $tRNA^{Phe}$ and RanGTP from *Saccharomyces cerevisiae* (Cook et al. 2009) (Figure 5). Xpot consists of 19 tandem HEAT repeats forming a large superhelix. HEAT repeats comprise a pair of α helices connected by a short loop. Due to the typical ~15° clockwise rotation between consecutive repeats, an arched superhelix is formed. Xpot features two such arches defined as N-terminal (repeats 1–9) and C-terminal (repeats 10–19). RanGTP mainly interacts with Xpot via HEATs 1 to 4 and HEAT9 in the N-terminal arch, while it also interacts with HEATs 13 and 17 of the C-terminal arch.

Xpot binds tRNA by wrapping around the acceptor arm and making contacts at the TΨC and D loop (elbow) (Figure 5, upper panels). Please note that the anticodon

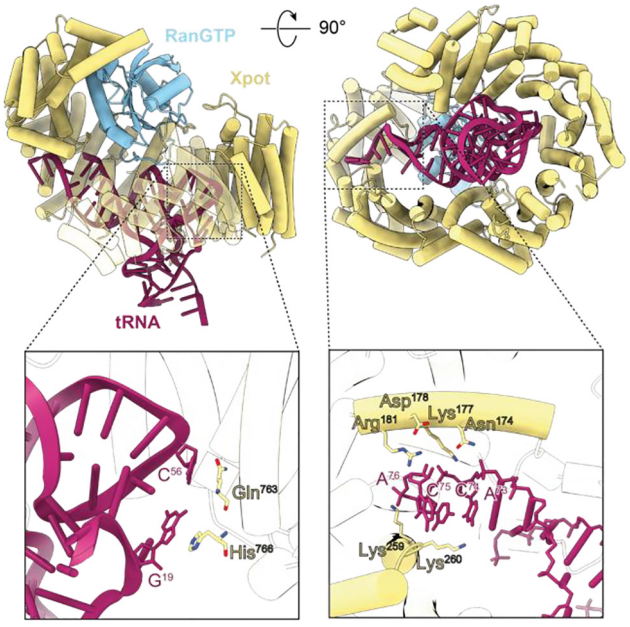


**Figure 5:** Structure of exportin-t with tRNA.
*S. pombe* exportin-t homologue Xpot forms a large superhelix due to its HEAT repeats, wrapping around the tRNA substrate. RanGTP triggers tRNA binding by conformational changes of Xpot, while it features only minor interactions with the tRNA acceptor stem. Essential stacking interactions of Xpot residues $His^{766}$ and $Gln^{763}$ with the $G^{19}$:$C^{56}$ base pair putatively probe tRNAs for their correct mature fold (lower left panel). At the termini, especially the CCA triplet binds to several conserved basic residues via ionic interactions with the phosphate backbone (lower right panel). Here, $Lys^{260}$ specifically interacts with the $C^{74}$ base and $C^{75}$ sugar. $Asn^{174}$ and $Asp^{176}$ hydrogen bond with the phosphate between $A^{73}$ and $C^{74}$ and the $A^{76}$ ribose, respectively. Additionally, $Asp^{176}$ possibly restricts the length of the 3′ terminus by preventing binding of additional phosphate groups (PDB ID 3ICQ).

arm of this minimal tRNA was mutated to a short tetraloop as it was considered dispensable for exportin-t interaction (Arts et al. 1998). Accordingly, only partial density can be observed for the tetraloop as it points away from the protein complex. The acceptor arm lies in a basic cleft formed by HEATs 8 to 18 and a small positively charged part of Ran which is driven by ionic interactions with the RNA phosphate backbone. The elbow of the tRNA binds the C-terminal arch of Xpot. Similar to the previously discussed proteins, a stacking interaction of the conserved $G^{19}$:$C^{56}$ base pair (numbering according to untruncated $tRNA^{Phe}$) with a histidine and glutamine is one of the key interactions between tRNA and Xpot (Figure 5, lower left panel). In fact, nuclear export is inhibited upon disruption of this base pair, indicating a tRNA folding surveillance step before export (Arts et al. 1998; Lipowsky et al. 1999). The RNA 5′-terminus protrudes between HEATs 6 to 8 and a positively charged patch of Ran. Interestingly, the structure reveals that uncleaved 5′-leaders would not fit into this tight pocket and thereby impairs export of unprocessed tRNAs. The 3′-CCA end is buried in a groove between HEATs 4 and 7 of Xpot (Figure 5, lower right panel). The interactions are mainly driven by contacts between conserved basic residues and the phosphate backbone of the CCA triplet. However, the amino acids also form hydrogen bonds with the sugars of the two cytosines. Another highly conserved aspartate is close to the 3′-OH of the terminal adenosine likely restricting the length of the 3′-terminus by repelling phosphate groups of additional nucleotides. As the last instance before tRNAs reach the cytosol, the export seems to be an especially tightly regulated quality control step for the cell.

## Transfer RNA splicing

Organisms of all three domains of life produce intron-containing precursor tRNAs (pre-tRNAs). However, the frequency of introns in tRNA genes varies greatly among organisms (Chan and Lowe 2016; Schmidt and Matera 2020). While humans and other vertebrates encode ~5–7% of tRNAs with introns, in baker's yeast and fission yeast over 20% of tRNAs are encoded with introns. Archaea are especially diverse ranging from ~6% in *Haloferax volcanii* to more than 50% in *Pyrobaculum aerophilum*. The removal of introns is essential for tRNAs to perform their key role in protein synthesis. This is particularly important for higher eukaryotes, as for example in humans some of the isodecoder families (tRNAs differing in sequence but share the same anticodon), like $tRNA^{Tyr}_{GTA}$ and $tRNA^{Ile}_{TAT}$, only exist as intron-containing precursors. Interestingly, bacteria encode self-splicing type I introns (Haugen et al. 2005; Reinhold-Hurek and Shub 1992) while Eukarya and Archaea rely on the coordinated activity of endonucleases, for intron cleavage, and ligases to join tRNA exon halves (Abelson et al. 1998).

Archaeal and eukaryotic endonucleases utilize somewhat different approaches for intron recognition. In Archaea, specific structural features at the exon–intron boundaries are recognized, whereas eukaryotic splicing endonucleases are proposed to use a molecular ruler mechanism (Schmidt and Matera 2020). This is likely due to the intron position in pre-tRNA. Although the canonical position in both, Eukarya and Archaea, is one nucleotide downstream of the anticodon (between nucleotides 37 and 38) (Figure 6A), introns can be found at virtually any position in archaeal tRNAs (Chan and Lowe 2016; Marck and Grosjean 2003; Sugahara et al. 2009). Noncanonical introns are also found in eukaryotes but seem to be restricted to tRNA pseudogenes (Chan and Lowe 2016). Archaeal tRNA introns form the bulge–helix–bulge (BHB) motif (Figure 6B), a structure consisting of a central four base pair helix flanked at each 3′ side by a single-stranded three–base bulge (Marck and Grosjean 2003). At the canonical position, the BHB motif positions the endonuclease cleavage sites within the bulges. Noteworthily, eukaryotic splicing endonucleases also recognize and cleave tRNA with the archaeal BHB motif (Di Segni et al. 2005; Fabbri et al. 1998). Yet, eukaryotes encode pre-tRNAs with BHB-like motifs having more variations in the central helix (Chan and Lowe 2016). Common features of the archaeal BHB motif are the positions of the cleavage sites in the single-stranded bulges. In contrast to Archaea, only a conserved interaction between a pyrimidine located six nucleotides upstream of the 5′ splice site with a purine three nucleotides upstream of the 3′ splice site seems to be important for efficient pre-tRNA cleavage (Baldi et al. 1992; Fabbri et al. 1998). As this represents an interaction between an anticodon base and an intron base, it was termed A-I base pair (Figure 6A). Recently, the importance of the A-I base pair was corroborated by biochemical studies with *Drosophila melanogaster* and human tRNA splicing endonuclease (TSEN) complex (Schmidt et al. 2019; Sekulovski et al. 2021).

All splicing endonucleases comprise two structural and two catalytic units which can appear in vastly different architectures. Archaeal splicing endonucleases can be classified into four types, $\alpha_4$, $\alpha'_2$, $(\alpha\beta)_2$, and $\varepsilon_2$ according to their subunit assembly. In contrast, eukaryotic splicing endonucleases have a heterotetrameric αβγδ architecture. Recently, *in vitro* analyses of the human TSEN complex corroborated the proposed subunit organizations of

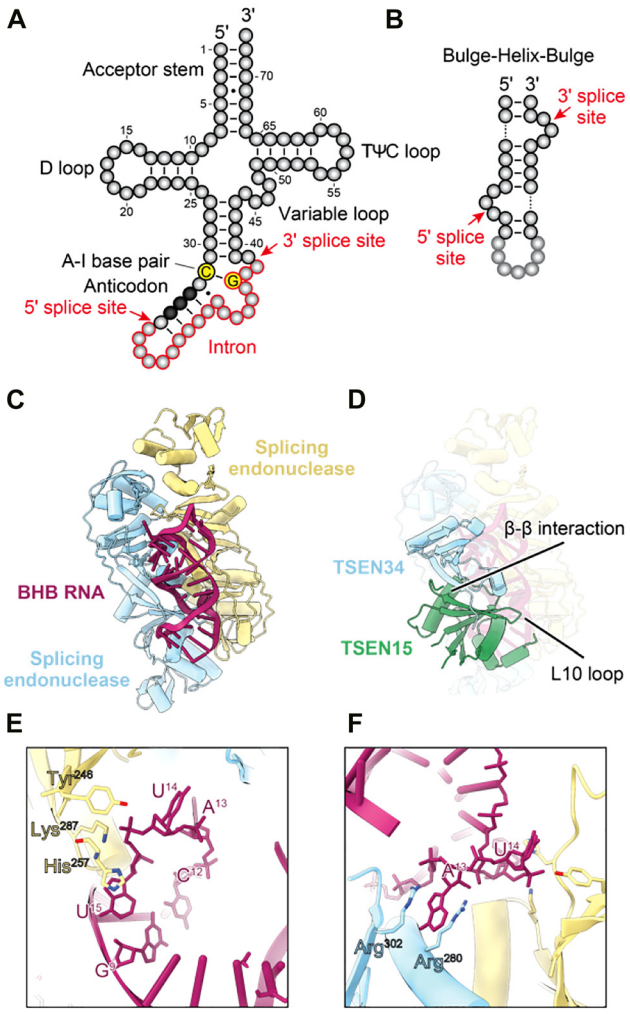


**Figure 6:** Structural basis of pre-tRNA splicing.
(A) Cloverleaf structure of an intron-containing pre-tRNA. In eukaryotes, pre-tRNAs form relaxed bulge–helix–bulge (BHB) motifs at the exon–intron boundaries. While the 3′ splice site usually retains the bulge, the 5′ splice site is more diverse in appearance. However, eukaryotic pre-tRNAs form a conserved interaction between a nucleotide from the anticodon stem (–6 from 5′ cleavage site) and a nucleotide in the intron (–3 from 3′ cleavage site), the so-called anticodon-intron or A-I base pair. (B) Classical BHB motif as found in Archaea. A central four base pair helix is flanked at the 3′ sites by three nucleotide bulges, with the cleavage sites residing between the second and third bulge nucleotide. (C) Structure of *A. fulgidus* splicing endonuclease dimer in complex with artificial BHB RNA substrate. The RNA binds symmetrically to the dimer interface. (D) Superposition of the human TSEN15-34 heterodimer with *A. fulgidus* splicing endonuclease. The β-β intersubunit interaction is conserved between archaeal and human complex. Although missing an interaction partner, the acidic L10 loop of TSEN15 is clearly visible, facing the subunit residing on the other splice site. (E) Interaction network of 5′ splice site. The catalytic $His^{257}$ stacks onto bulge base $A^{15}$ which in effect hydrogen bonds with the minor groove of the $G^{9}$:$C^{12}$ base pair. This positions the scissile phosphate between $U^{14}$ and $A^{15}$ in the centre of the catalytic triad $Tyr^{246}$, $His^{257}$, and $Lys^{287}$. (F) 5′ splice site cation-π-sandwich. $Arg^{280}$ and $Arg^{302}$ of subunit A act as a molecular tweezer on the nucleobase $A^{13}$, pinching out the nucleotide via stacking and hence positioning the bulge for cleavage at subunit B (PDB ID 2GJW, 6Z9U).

TSEN15 and TSEN54 as structural subunits and TSEN2 and TSEN34 as the 5′ and 3′ cleaving subunits, respectively (Hayne et al. 2020; Sekulovski et al. 2021). The crystal structure of homotetrameric *Methanocaldococcus jannaschii* $\alpha_4$-type endonuclease revealed two main intersubunit contacts: a pair of hydrophobic antiparallel β strands of two neighbouring α subunits and ionic interactions between an acidic L10 loop of one subunit with a basic pocket of an opposing α subunit. These structural elements are conserved in all four types of archaeal endonucleases and were also proposed for eukaryotic endonucleases. Indeed, we could recently verify the conserved architecture for human TSEN by obtaining a crystal structure for a TSEN15-34 subcomplex (Sekulovski et al. 2021) (Figure 6D).

A crystal structure of an $\alpha'_2$-type endonuclease from *Archaeoglobus fulgidus* in complex with a synthetic BHB RNA oligonucleotide describes binding and cleavage mechanism of intron-containing pre-tRNA (Xue et al. 2006) (Figure 6C). The endonuclease binds the RNA symmetrically at the central surface between its two subunits interacting via three arginines and a histidine with the bulge nucleotides in a sequence-independent fashion. The key feature is the so-called cross-subunit cation-π-sandwich. At both cleavage sites, the nucleobase of the first bulge nucleotide is pinched by an arginine tweezer of the subunit in trans interacting via the π-stacking effect (Figure 6F). Interestingly, although this motif is also conserved in eukaryotes, alanine substitutions only affect 5′ cleavage (Trotta et al. 2006). In the archaeal complex, the catalytic histidine residue stacks with the adenine base of the third bulge nucleotide to position it in an extensive hydrogen network with the 3′ terminal base pair of the central BHB helix. This drastically changes the geometry of the scissile phosphate at both cleavage sites facilitating an $S_N2$-type in-line attack of the 2′ oxygen. At the active site, the universally conserved residues tyrosine, histidine, and lysine catalyse the RNase A-like mechanism of cleavage (Figure 6E). $Tyr^{246}$ deprotonates the nucleophilic 2′ oxygen, $His^{257}$ protonates the leaving 5′ oxygen, and $Lys^{287}$ stabilizes the transition state.

The pioneering work on *A. fulgidus* splicing endonuclease provides insights into BHB motif interactions and cleavage mechanism for eukaryotic endonucleases but cannot explain how cleavage sites are recognized in more relaxed BHB motifs. Intron-containing yeast pre-tRNAs were shown to retain their tertiary structure in the TΨC-arm, D-arm, and acceptor stem (Lee and Knapp 1985; Swerdlow and Guthrie 1984). Together with the notion that eukaryotic tRNA introns are invariably inserted at the canonical position, it was proposed that, in eukaryotes, endonucleases recognize the mature body and position their catalytic subunits at the cleavage sites by a molecular ruler mechanism (Greer et al. 1987; Reyes and Abelson 1988).

Pre-tRNA intron cleavage produces a 5′ exon with a 2′–3′ cyclic phosphate, a 3′ exon with a 5′ hydroxyl, and an intron with a 5′ hydroxyl and a 2′–3′ cyclic phosphate. The exon halves need to be religated for the maturation of the tRNA (Schmidt et al. 2019; Schmidt and Matera 2020). While yeast and plants utilize an additional phosphorylation of the 3′ exon, the 5′ phosphate ligation pathway, metazoans and Archaea make direct use of the 2′–3′ cyclic phosphate of the 5′ exon, called 3′ phosphate ligation pathway. Noteworthy, most of the enzymes for the 5′ phosphate ligation pathway are also present in vertebrates, but a corresponding ligase has so far not been identified (Kurihara et al. 1987; Kurihara et al. 1988; Spinelli et al. 1998; Vogel and Thompson 1987; Weitzer and Martinez 2007). Strikingly, the human TSEN complex associates with the RNA kinase CLP1 which was assigned to the putative 5′ phosphate ligation pathway (Paushkin et al. 2004; Weitzer and Martinez 2007). Here, we focus on the 3′ phosphate ligation pathway and refer to these excellent reviews for a complete overview on tRNA ligation (Popow et al. 2012; Yoshihisa 2014). The RtcB homologue HSPC117, a 3′ phosphate ligase, has been identified as the key enzyme in humans (Popow et al. 2011). First, the 2′–3′ cyclic phosphate is opened by a not yet identified cyclic phosphodiesterase, resulting in a 3′ phosphorylated 5′ exon. HSPC117 needs to be activated by the small protein "Archease" via enhancement of a GMP transfer from GTP to the HSPC117 active site. Afterwards, HSPC117 acts together with the RNA helicase DDX1 to transfer the GMP moiety to the 3′ phosphate of the 5′ exon. This enables HSPC117 to perform the ligation reaction to the 3′–5′ phosphodiester yielding the mature tRNA molecule. Albeit the architecture of the tRNA ligase complex has been described recently (Kroupova et al. 2021), no high-resolution structures of HSPC117 or other RtcB homologues in complex with tRNA exons are available. However, structural analyses of the *Pyrococcus horikoshii* RtcB revealed key residues for $Mn^{2+}$ coordination, GMP transfer and putative RNA interaction (Banerjee et al. 2021; Englert et al. 2012). A central cysteine binds both manganese ions and is believed to confer the reported oxidation sensitivity of the human tRNA ligase complex (Asanovic et al. 2021; Banerjee et al. 2021). The GMP moiety is first transferred to a conserved histidine residue which guanylylates the 5′ exon in a $Mn^{2+}$-dependent manner. This activation step is not fully understood as RtcB has been shown to ligate RNA with both, 3′ phosphates and 2′–3′ cyclic phosphates, with 5′ hydroxyl RNA (Popow et al. 2011; Tanaka et al. 2011). Interestingly, bacterial RtcB catalyses the cleavage of the 2′–3′ cyclic phosphate to a 3′ phosphate before the actual ligation reaction (Tanaka et al. 2011). This implies a similar mechanism for the human tRNA ligase complex and would reveal the identity of the missing cyclic phosphodiesterase. In future studies, high-resolution structures of the human tRNA ligase complex bound to tRNA exons will certainly clarify these ambiguities.

## Transfer RNA processing and neurodevelopmental diseases

The processing of tRNA is a diverse cascade of reactions at multiple intracellular locations (Figure 7). Consequently, a plethora of possibilities exists for mutations to occur within tRNAs or tRNA processing and modifying enzymes. It comes with a surprise that most occurring mutations cause severe neurological disorders affecting particular brain regions while other tissues seem largely unaffected, a phenomenon coined selective vulnerability (Fu et al. 2018; Schaffer et al. 2019). tRNA associated neurological pathologies can be broadly divided in five categories: mitochondrial encephalomyopathies, Charcot–Marie–Tooth disease, leukodystrophy, pontocerebellar hypoplasia, and intellectual disability syndromes (Schaffer et al. 2019). The symptoms are as diverse as the underlying diseases including for example myopathy, progressive microcephaly, dyskinesia, and mental retardation. Why do tRNA associated mutations focus on selective tissue although tRNA is ubiquitously expressed? What are the molecular mechanisms leading to these pathologies, specifically in neurons? The ongoing list of publications connecting tRNA with neurodevelopmental diseases sparked these interesting and yet complex questions (Kirchner and Ignatova 2015; Schaffer et al. 2019). We discuss possible answers using the example of pontocerebellar hypoplasia and draw parallels to other neurological diseases.

Mutations in any subunit of human TSEN and CLP1 have been identified to cause pontocerebellar hypoplasia (PCH) (Budde et al. 2008; Bierhals et al. 2013; Breuss et al. 2016; Kasher et al. 2011; Karaca et al. 2014; Schaffer et al. 2014). We could show that the most common mutation affecting the TSEN54 subunit reduces complex stability and pre-tRNA splicing in PCH patient-derived fibroblasts (Sekulovski et al. 2021). Similarly, we observed higher temperature sensitivity for all mutant TSEN complexes *in vitro*. However, overall pre-tRNA levels were only mildly increased in patient cells. While this might have minimal effects in other tissue, neurons could be more susceptible to small alterations of tRNA equilibria. As cells with high demand for rapid protein biosynthesis, neurons could suffer from even slightly disbalanced levels of tRNAs. Supporting this theory, recent studies with Charcot–Marie–Tooth mouse models reported reduced levels of

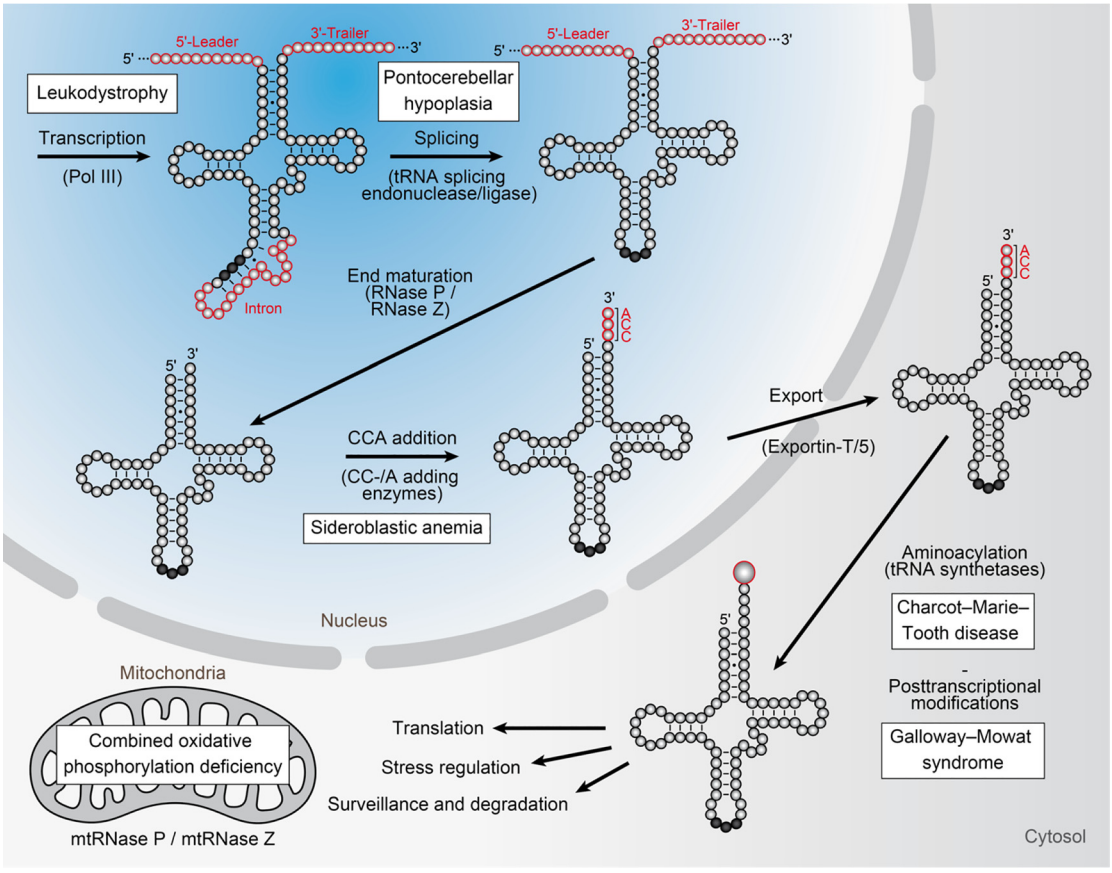


**Figure 7:** Transfer RNA processing and disease.
After transcription by RNA polymerase III (Pol III), precursor tRNAs undergo several essential processing steps for maturation. Note that the order of these events as depicted in the figure is not entirely fixed and varies among transcripts and organisms. For higher eukaryotes, 5′ and 3′ end maturation, CCA addition, and intron splicing likely occur in the nucleus. Exportin-t thoroughly probes mature tRNA before export to the cytosol where aminoacylation and nucleobase modifications are performed. Here, tRNAs can fulfil their canonical role as key players in protein synthesis by delivering amino acids to translating ribosomes. More recently, tRNAs were also connected to other cellular processes regulating stress response and neuroprotection (see text). Aberrations in tRNA transcription and processing are tightly connected with a list of neurological diseases including leukodystrophy (Online Mendelian Inheritance in Man [OMIM]: 607694, 614381), pontocerebellar hypoplasia (OMIM: 615803, 612389, 612390, 617026, 225753), combined oxidative phosphorylation deficiency (OMIM: 615440), sideroblastic anaemia (OMIM: 616084), Charcot–Marie–Tooth disease (OMIM: 613287, 616280, 616625, 608323, 613641, 601472), and Galloway–Mowat syndrome (OMIM: 617729).

$tRNA^{Gly}$ leading to ribosome stalling and triggering of the integrated stress response in motor neurons (Spaulding et al. 2021; Zuko et al. 2021).

Alternatively, splicing of neuron-specific pre-tRNAs could be aberrant. Expression profiles of tRNA isodecoder families can vary tremendously among different tissues and during development and were shown to be altered in certain diseases (Dittmar et al. 2006; Gingold et al. 2014; Goodarzi et al. 2016; Schmitt et al. 2014). Correspondingly, a mouse study demonstrated how a mutated central nervous system-specific tRNA gene caused ribosome stalling and consecutive neurodegeneration (Ishimura et al. 2014).

Another interesting explanation for neurodegeneration is the occurrence of erroneous tRNA-derived fragments, a class of non-coding RNAs regulating translation, gene expression, silencing, and neuroprotection (Anderson and Ivanov 2014; Thompson and Parker 2009). Both, a loss-of-function or gain-of-function mechanism could be feasible. Indeed, recent results indicate that 5′ fragments derived from $pre\text{-}tRNA^{Tyr}$ cause neuronal cell death and microcephaly in a p53-dependent manner (Inoue et al. 2020). Similarly, a loss or gain of function for TSEN (and other processing enzymes) could potentially produce yet unknown neurotoxic RNAs or deplete neuroprotective RNAs by processing of non-canonical targets. In yeast, TSEN has already been associated with mRNA decay and non-canonical mRNA splicing, opening new pathways to be explored in humans (Cherry et al. 2018; Dhungel and Hopper 2012; Hurtig et al. 2021; Tsuboi et al. 2015).

## Closing remarks

Despite great biological and medical advances in analysing and treating neurological diseases, their majority poses a mystery for science and even a threat for some. With emphasis on PCH, we presented putative mechanisms for disease development and how erroneous (pre-)tRNA processing can cause neurodegeneration. Improving the understanding of one neurological disease could unravel general pathological principles. For PCH, the structural basis to understand most of the TSEN/CLP1 mutations is still missing. Not only would a high-resolution structure of TSEN/CLP1 with substrate pre-tRNA improve our understanding of PCH-causing mutations, but it would also present a great opportunity for drug design and treatment rationales. Similarly, structural information about other mutations causing neurological disorders will clearly advance the field. Although we presented different theories about the onset of neurodegeneration, it should be noted that several mechanisms could act in parallel or depend on a specific type of disease emerging only in specific cell types. Future studies will unravel the putatively diverse pathways causing neurodevelopmental diseases and enable development of entirely novel therapeutic approaches.

**Author contributions:** All authors have accepted responsibility for the entire content of this submitted manuscript and approved submission.
**Research funding:** This work was financially supported by the German Research Foundation (DFG, grant number TR 1711/1-7), the Collaborative Research Center 902 (SFB902) 'Molecular Principles of RNA-based Regulation', and the Boehringer Ingelheim Fonds.
**Conflict of interest statement:** The authors declare no conflicts of interest regarding this article.

## References

Abelson, J., Trotta, C.R., and Li, H. (1998). tRNA splicing. J. Biol. Chem. 273: 12685–12688.

Anderson, P. and Ivanov, P. (2014). tRNA fragments in human health and disease. FEBS Lett. 588: 4297–4304.

Arts, G.J., Kuersten, S., Romby, P., Ehresmann, B., and Mattaj, I.W. (1998). The role of exportin-t in selective nuclear export of mature tRNAs. EMBO J. 17: 7430–7441.

Asanovic, I., Strandback, E., Kroupova, A., Pasajlic, D., Meinhart, A., Tsung-Pin, P., Djokovic, N., Anrather, D., Schuetz, T., Suskiewicz, M.J., et al. (2021). The oxidoreductase PYROXD1 uses $NAD(P)^+$ as an antioxidant to sustain tRNA ligase activity in pre-tRNA splicing and unfolded protein response. Mol. Cell 81: 2520–2532.e16.

Augustin, M.A., Reichert, A.S., Betat, H., Huber, R., Morl, M., and Steegborn, C. (2003). Crystal structure of the human CCA-adding enzyme: insights into template-independent polymerization. J. Mol. Biol. 328: 985–994.

Baldi, M.I., Mattoccia, E., Bufardeci, E., Fabbri, S., and Tocchini-Valentini, G.P. (1992). Participation of the intron in the reaction catalyzed by the *Xenopus* tRNA splicing endonuclease. Science 255: 1404–1408.

Banerjee, A., Goldgur, Y., and Shuman, S. (2021). Structure of 3'-PO4/5'-OH RNA ligase RtcB in complex with a 5'-OH oligonucleotide. RNA. https://doi.org/10.1261/rna.078692.121.

Bhatta, A., Dienemann, C., Cramer, P., and Hillen, H.S. (2021). Structural basis of RNA processing by human mitochondrial RNase P. Nat. Struct. Mol. Biol. 28: 713–723.

Bierhals, T., Korenke, G.C., Uyanik, G., and Kutsche, K. (2013). Pontocerebellar hypoplasia type 2 and TSEN2: review of the literature and two novel mutations. Eur. J. Med. Genet. 56: 325–330.

Breuss, M.W., Sultan, T., James, K.N., Rosti, R.O., Scott, E., Musaev, D., Furia, B., Reis, A., Sticht, H., Al-Owain, M., et al. (2016). Autosomal-recessive mutations in the tRNA splicing endonuclease subunit TSEN15 cause pontocerebellar hypoplasia and progressive microcephaly. Am. J. Hum. Genet. 99: 785.

Budde, B.S., Namavar, Y., Barth, P.G., Poll-The, B.T., Nurnberg, G., Becker, C., Van Ruissen, F., Weterman, M.A., Fluiter, K., Te Beek, E.T., et al. (2008). tRNA splicing endonuclease mutations cause pontocerebellar hypoplasia. Nat. Genet. 40: 1113–1118.

Calado, A., Treichel, N., Muller, E.C., Otto, A., and Kutay, U. (2002). Exportin-5-mediated nuclear export of eukaryotic elongation factor 1A and tRNA. EMBO J. 21: 6216–6224.

Cameron, A.D., Ridderstrom, M., Olin, B., Kavarana, M.J., Creighton, D.J., and Mannervik, B. (1999a). Reaction mechanism of glyoxalase I explored by an X-ray crystallographic analysis of the human enzyme in complex with a transition state analogue. Biochemistry 38: 13480–13490.

Cameron, A.D., Ridderstrom, M., Olin, B., and Mannervik, B. (1999b). Crystal structure of human glyoxalase II and its complex with a glutathione thiolester substrate analogue. Structure 7: 1067–1078.

Chan, P.P. and Lowe, T.M. (2016). GtRNAdb 2.0: an expanded database of transfer RNA genes identified in complete and draft genomes. Nucleic Acids Res. 44: D184–D189.

Chatterjee, K., Nostramo, R.T., Wan, Y., and Hopper, A.K. (2018). tRNA dynamics between the nucleus, cytoplasm and mitochondrial surface: location, location, location. Biochim. Biophys. Acta Gene Regul. Mech. 1861: 373–386.

Cherry, P.D., White, L.K., York, K., and Hesselberth, J.R. (2018). Genetic bypass of essential RNA repair enzymes in budding yeast. RNA 24: 313–323.

Cook, A.G., Fukuhara, N., Jinek, M., and Conti, E. (2009). Structures of the tRNA export factor in the nuclear and cytosolic states. Nature 461: 60–65.

Copela, L.A., Fernandez, C.F., Sherrer, R.L., and Wolin, S.L. (2008). Competition between the Rex1 exonuclease and the La protein affects both Trf4p-mediated RNA quality control and pre-tRNA maturation. RNA 14: 1214–1227.

Coughlin, D.J., Pleiss, J.A., Walker, S.C., Whitworth, G.B., and Engelke, D.R. (2008). Genome-wide search for yeast RNase P substrates reveals role in maturation of intron-encoded box C/D small nucleolar RNAs. Proc. Natl. Acad. Sci. U.S.A. 105: 12218–12223.

Dhungel, N. and Hopper, A.K. (2012). Beyond tRNA cleavage: novel essential function for yeast tRNA splicing endonuclease unrelated to tRNA processing. Genes Dev. 26: 503–514.

Di Segni, G., Borghese, L., Sebastiani, S., and Tocchini-Valentini, G.P. (2005). A pre-tRNA carrying intron features typical of Archaea is spliced in yeast. RNA 11: 70–76.

Dittmar, K.A., Goodenbour, J.M., and Pan, T. (2006). Tissue-specific differences in human transfer RNA expression. PLoS Genet. 2: e221.

Ellis, J.C. and Brown, J.W. (2009). The RNase P family. RNA Biol. 6: 362–369.

Englert, M., Xia, S., Okada, C., Nakamura, A., Tanavde, V., Yao, M., Eom, S.H., Konigsberg, W.H., Soll, D., and Wang, J. (2012). Structural and mechanistic insights into guanylylation of RNA-splicing ligase RtcB joining RNA between 3′-terminal phosphate and 5′-OH. Proc. Natl. Acad. Sci. U.S.A. 109: 15235–15240.

Esakova, O. and Krasilnikov, A.S. (2010). Of proteins and RNA: the RNase P/MRP family. RNA 16: 1725–1747.

Fabbri, S., Fruscoloni, P., Bufardeci, E., Di Nicola Negri, E., Baldi, M.I., Attardi, D.G., Mattoccia, E., and Tocchini-Valentini, G.P. (1998). Conservation of substrate recognition mechanisms by tRNA splicing endonucleases. Science 280: 284–286.

Fu, H., Hardy, J., and Duff, K.E. (2018). Selective vulnerability in neurodegenerative diseases. Nat. Neurosci. 21: 1350–1358.

Gingold, H., Tehler, D., Christoffersen, N.R., Nielsen, M.M., Asmar, F., Kooistra, S.M., Christophersen, N.S., Christensen, L.L., Borre, M., Sorensen, K.D., et al. (2014). A dual program for translation regulation in cellular proliferation and differentiation. Cell 158: 1281–1292.

Goodarzi, H., Nguyen, H.C.B., Zhang, S., Dill, B.D., Molina, H., and Tavazoie, S.F. (2016). Modulated expression of specific tRNAs drives gene expression and cancer progression. Cell 165: 1416–1427.

Gray, M.W. and Gopalan, V. (2020). Piece by piece: building a ribozyme. J. Biol. Chem. 295: 2313–2323.

Green, R. and Noller, H.F. (1997). Ribosomes and translation. Annu. Rev. Biochem. 66: 679–716.

Greer, C.L., Soll, D., and Willis, I. (1987). Substrate recognition and identification of splice sites by the tRNA-splicing endonuclease and ligase from *Saccharomyces cerevisiae*. Mol. Cell Biol. 7: 76–84.

Guerrier-Takada, C. and Altman, S. (1984). Catalytic activity of an RNA molecule prepared by transcription *in vitro*. Science 223: 285–286.

Guerrier-Takada, C., Gardiner, K., Marsh, T., Pace, N., and Altman, S. (1983). The RNA moiety of ribonuclease P is the catalytic subunit of the enzyme. Cell 35: 849–857.

Han, L. and Phizicky, E.M. (2018). A rationale for tRNA modification circuits in the anticodon loop. RNA 24: 1277–1284.

Haugen, P., Simon, D.M., and Bhattacharya, D. (2005). The natural history of group I introns. Trends Genet. 21: 111–119.

Hayne, C.K., Schmidt, C.A., Haque, M.I., Matera, A.G., and Stanley, R.E. (2020). Reconstitution of the human tRNA splicing endonuclease complex: insight into the regulation of pre-tRNA cleavage. Nucleic Acids Res. 48: 7609–7622.

Holzmann, J., Frank, P., Loffler, E., Bennett, K.L., Gerner, C., and Rossmanith, W. (2008). RNase P without RNA: identification and functional reconstitution of the human mitochondrial tRNA processing enzyme. Cell 135: 462–474.

Hopper, A.K. and Nostramo, R.T. (2019). tRNA processing and subcellular trafficking proteins multitask in pathways for other RNAs. Front. Genet. 10: 96.

Hurtig, J.E., Steiger, M.A., Nagarajan, V.K., Li, T., Chao, T.C., Tsai, K.L., and Van Hoof, A. (2021). Comparative parallel analysis of RNA ends identifies mRNA substrates of a tRNA splicing endonuclease-initiated mRNA decay pathway. Proc. Natl. Acad. Sci. U.S.A. 118, https://doi.org/10.1073/pnas.2020429118.

Inoue, M., Hada, K., Shiraishi, H., Yatsuka, H., Fujinami, H., Morisaki, I., Nishida, Y., Matsubara, E., Ishitani, T., Hanada, R., et al. (2020). Tyrosine pre-transfer RNA fragments are linked to p53-dependent neuronal cell death via PKM2. Biochem. Biophys. Res. Commun. 525: 726–732.

Ishii, R., Minagawa, A., Takaku, H., Takagi, M., Nashimoto, M., and Yokoyama, S. (2005). Crystal structure of the tRNA 3′ processing endoribonuclease tRNase Z from *Thermotoga maritima*. J. Biol. Chem. 280: 14138–14144.

Ishimura, R., Nagy, G., Dotu, I., Zhou, H., Yang, X.L., Schimmel, P., Senju, S., Nishimura, Y., Chuang, J.H., and Ackerman, S.L. (2014). RNA function. Ribosome stalling induced by mutation of a CNS-specific tRNA causes neurodegeneration. Science 345: 455–459.

Karaca, E., Weitzer, S., Pehlivan, D., Shiraishi, H., Gogakos, T., Hanada, T., Jhangiani, S.N., Wiszniewski, W., Withers, M., Campbell, I.M., et al. (2014). Human CLP1 mutations alter tRNA biogenesis, affecting both peripheral and central nervous system function. Cell 157: 636–650.

Kasher, P.R., Namavar, Y., Van Tijn, P., Fluiter, K., Sizarov, A., Kamermans, M., Grierson, A.J., Zivkovic, D., and Baas, F. (2011). Impairment of the tRNA-splicing endonuclease subunit 54 (tsen54) gene causes neurological abnormalities and larval death in zebrafish models of pontocerebellar hypoplasia. Hum. Mol. Genet. 20: 1574–1584.

Kim, D.F. and Green, R. (1999). Base-pairing between 23S rRNA and tRNA in the ribosomal A site. Mol. Cell 4: 859–864.

Kim, S.H., Quigley, G.J., Suddath, F.L., McPherson, A., Sneden, D., Kim, J.J., Weinzierl, J., and Rich, A. (1973). Three-dimensional structure of yeast phenylalanine transfer RNA: folding of the polynucleotide chain. Science 179: 285–288.

Kirchner, S. and Ignatova, Z. (2015). Emerging roles of tRNA in adaptive translation, signalling dynamics and disease. Nat. Rev. Genet. 16: 98–112.

Kirsebom, L.A. and Trobro, S. (2009). RNase P RNA-mediated cleavage. IUBMB Life 61: 189–200.

Komine, Y., Kitabatake, M., Yokogawa, T., Nishikawa, K., and Inokuchi, H. (1994). A tRNA-like structure is present in 10Sa RNA, a small stable RNA from *Escherichia coli*. Proc. Natl. Acad. Sci. U.S.A. 91: 9223–9227.

Kramer, E.B. and Hopper, A.K. (2013). Retrograde transfer RNA nuclear import provides a new level of tRNA quality control in *Saccharomyces cerevisiae*. Proc. Natl. Acad. Sci. U.S.A. 110: 21042–21047.

Kroupova, A., Ackle, F., Asanovic, I., Weitzer, S., Boneberg, F.M., Faini, M., Leitner, A., Chui, A., Aebersold, R., Martinez, J., et al. (2021). Molecular architecture of the human tRNA ligase complex. Elife 10, https://doi.org/10.7554/elife.71656.

Krutyholowa, R., Zakrzewski, K., and Glatt, S. (2019). Charging the code – tRNA modification complexes. Curr. Opin. Struct. Biol. 55: 138–146.

Kufel, J. and Tollervey, D. (2003). 3′-processing of yeast tRNATrp precedes 5′-processing. RNA 9: 202–208.

Kurihara, T., Fowler, A.V., and Takahashi, Y. (1987). cDNA cloning and amino acid sequence of bovine brain 2′, 3′-cyclic-nucleotide 3′-phosphodiesterase. J. Biol. Chem. 262: 3256–3261.

Kurihara, T., Takahashi, Y., Nishiyama, A., and Kumanishi, T. (1988). cDNA cloning and amino acid sequence of human brain 2′, 3′-cyclic-nucleotide 3′-phosphodiesterase. Biochem. Biophys. Res. Commun. 152: 837–842.

Kutay, U., Lipowsky, G., Izaurralde, E., Bischoff, F.R., Schwarzmaier, P., Hartmann, E., and Gorlich, D. (1998). Identification of a tRNA-specific nuclear export receptor. Mol. Cell 1: 359–369.

Lechner, M., Rossmanith, W., Hartmann, R.K., Tholken, C., Gutmann, B., Giege, P., and Gobert, A. (2015). Distribution of ribonucleoprotein and protein-only RNase P in Eukarya. Mol. Biol. Evol. 32: 3186–3193.

Lee, M.C. and Knapp, G. (1985). Transfer RNA splicing in *Saccharomyces cerevisiae*. Secondary and tertiary structures of the substrates. J. Biol. Chem. 260: 3108–3115.

Li De La Sierra-Gallay, I., Mathy, N., Pellegrini, O., and Condon, C. (2006). Structure of the ubiquitous 3′ processing enzyme RNase Z bound to transfer RNA. Nat. Struct. Mol. Biol. 13: 376–377.

Li De La Sierra-Gallay, I., Pellegrini, O., and Condon, C. (2005). Structural basis for substrate binding, cleavage and allostery in the tRNA maturase RNase Z. Nature 433: 657–661.

Lipowsky, G., Bischoff, F.R., Izaurralde, E., Kutay, U., Schafer, S., Gross, H.J., Beier, H., and Gorlich, D. (1999). Coordination of tRNA nuclear export with processing of tRNA. RNA 5: 539–549.

Liu, J.C., Liu, M., and Horowitz, J. (1998). Recognition of the universally conserved 3′-CCA end of tRNA by elongation factor EF-Tu. RNA 4: 639–646.

Lizano, E., Scheibe, M., Rammelt, C., Betat, H., and Morl, M. (2008). A comparative analysis of CCA-adding enzymes from human and *E. coli*: differences in CCA addition and tRNA 3′-end repair. Biochimie 90: 762–772.

Maraia, R.J. and Lamichhane, T.N. (2011). 3′ processing of eukaryotic precursor tRNAs. Wiley Interdiscip. Rev. RNA 2: 362–375.

Marck, C. and Grosjean, H. (2003). Identification of BHB splicing motifs in intron-containing tRNAs from 18 archaea: evolutionary implications. RNA 9: 1516–1531.

Nissen, P., Hansen, J., Ban, N., Moore, P.B., and Steitz, T.A. (2000). The structural basis of ribosome activity in peptide bond synthesis. Science 289: 920–930.

Nostramo, R.T. and Hopper, A.K. (2020). A novel assay provides insight into tRNAPhe retrograde nuclear import and re-export in *S. cerevisiae*. Nucleic Acids Res. 48: 11577–11588.

O'connor, J.P. and Peebles, C.L. (1991). In vivo pre-tRNA processing in *Saccharomyces cerevisiae*. Mol. Cell Biol. 11: 425–439.

Ozanick, S.G., Wang, X., Costanzo, M., Brost, R.L., Boone, C., and Anderson, J.T. (2009). Rex1p deficiency leads to accumulation of precursor initiator tRNAMet and polyadenylation of substrate RNAs in *Saccharomyces cerevisiae*. Nucleic Acids Res. 37: 298–308.

Palazzo, A.F. and Lee, E.S. (2015). Non-coding RNA: what is functional and what is junk? Front. Genet. 6: 2.

Paushkin, S.V., Patel, M., Furia, B.S., Peltz, S.W., and Trotta, C.R. (2004). Identification of a human endonuclease complex reveals a link between tRNA splicing and pre-mRNA 3′ end formation. Cell 117: 311–321.

Pellegrini, O., Nezzar, J., Marchfelder, A., Putzer, H., and Condon, C. (2003). Endonucleolytic processing of CCA-less tRNA precursors by RNase Z in *Bacillus subtilis*. EMBO J. 22: 4534–4543.

Popow, J., Englert, M., Weitzer, S., Schleiffer, A., Mierzwa, B., Mechtler, K., Trowitzsch, S., Will, C.L., Luhrmann, R., Soll, D., et al. (2011). HSPC117 is the essential subunit of a human tRNA splicing ligase complex. Science 331: 760–764.

Popow, J., Schleiffer, A., and Martinez, J. (2012). Diversity and roles of (t)RNA ligases. Cell. Mol. Life Sci. 69: 2657–2670.

Redko, Y., Li De La Sierra-Gallay, I., and Condon, C. (2007). When all's zed and done: the structure and function of RNase Z in prokaryotes. Nat. Rev. Microbiol. 5: 278–286.

Reinhold-Hurek, B. and Shub, D.A. (1992). Self-splicing introns in tRNA genes of widely divergent bacteria. Nature 357: 173–176.

Reiter, N.J., Osterman, A., Torres-Larios, A., Swinger, K.K., Pan, T., and Mondragon, A. (2010). Structure of a bacterial ribonuclease P holoenzyme in complex with tRNA. Nature 468: 784–789.

Reyes, V.M. and Abelson, J. (1988). Substrate recognition and splice site determination in yeast tRNA splicing. Cell 55: 719–730.

Rich, A. and Rajbhandary, U.L. (1976). Transfer RNA: molecular structure, sequence, and properties. Annu. Rev. Biochem. 45: 805–860.

Schaffer, A.E., Eggens, V.R., Caglayan, A.O., Reuter, M.S., Scott, E., Coufal, N.G., Silhavy, J.L., Xue, Y., Kayserili, H., Yasuno, K., et al. (2014). CLP1 founder mutation links tRNA splicing and maturation to cerebellar development and neurodegeneration. Cell 157: 651–663.

Schaffer, A.E., Pinkard, O., and Coller, J.M. (2019). tRNA metabolism and neurodevelopmental disorders. Annu. Rev. Genom. Hum. Genet. 20: 359–387.

Schencking, I., Rossmanith, W., and Hartmann, R.K. (2020). Diversity and evolution of RNase P. In: Pontarotti, P. (Ed.). *Evolutionary biology—a transdisciplinary approach*. Cham: Springer.

Schiffer, S., Rosch, S., and Marchfelder, A. (2002). Assigning a function to a conserved group of proteins: the tRNA 3′-processing enzymes. EMBO J. 21: 2769–2777.

Schilling, O., Spath, B., Kostelecky, B., Marchfelder, A., Meyer-Klaucke, W., and Vogel, A. (2005). Exosite modules guide substrate recognition in the ZiPD/ElaC protein family. J. Biol. Chem. 280: 17857–17862.

Schimmel, P. (2018). The emerging complexity of the tRNA world: mammalian tRNAs beyond protein synthesis. Nat. Rev. Mol. Cell Biol. 19: 45–58.

Schmidt, C.A., Giusto, J.D., Bao, A., Hopper, A.K., and Matera, A.G. (2019). Molecular determinants of metazoan tricRNA biogenesis. Nucleic Acids Res. 47: 6452–6465.

Schmidt, C.A. and Matera, A.G. (2020). tRNA introns: presence, processing, and purpose. Wiley Interdiscip. Rev. RNA 11: e1583.

Schmitt, B.M., Rudolph, K.L., Karagianni, P., Fonseca, N.A., White, R.J., Talianidis, I., Odom, D.T., Marioni, J.C., and Kutter, C. (2014). High-resolution mapping of transcriptional dynamics across tissue development reveals a stable mRNA-tRNA interface. Genome Res. 24: 1797–1807.

Sekulovski, S., Devant, P., Panizza, S., Gogakos, T., Pitiriciu, A., Heitmeier, K., Ramsay, E.P., Barth, M., Schmidt, C., Tuschl, T., et al. (2021). Assembly defects of human tRNA splicing endonuclease contribute to impaired pre-tRNA processing in pontocerebellar hypoplasia. Nat. Commun. 12: 5610.

Spaulding, E.L., Hines, T.J., Bais, P., Tadenev, A.L.D., Schneider, R., Jewett, D., Pattavina, B., Pratt, S.L., Morelli, K.H., Stum, M.G., et al. (2021). The integrated stress response contributes to tRNA

synthetase-associated peripheral neuropathy. Science 373: 1156–1161.

Spinelli, S.L., Malik, H.S., Consaul, S.A., and Phizicky, E.M. (1998). A functional homolog of a yeast tRNA splicing enzyme is conserved in higher eukaryotes and in *Escherichia coli*. Proc. Natl. Acad. Sci. U.S.A. 95: 14136–14141.

Sprinzl, M. and Cramer, F. (1979). The -C-C-A end of tRNA and its role in protein biosynthesis. Prog. Nucleic Acid Res. Mol. Biol. 22: 1–69.

Sugahara, J., Fujishima, K., Morita, K., Tomita, M., and Kanai, A. (2009). Disrupted tRNA gene diversity and possible evolutionary scenarios. J. Mol. Evol. 69: 497–504.

Suzuki, T. (2021). The expanding world of tRNA modifications and their disease relevance. Nat. Rev. Mol. Cell Biol. 22: 375–392.

Swerdlow, H. and Guthrie, C. (1984). Structure of intron-containing tRNA precursors. Analysis of solution conformation using chemical and enzymatic probes. J. Biol. Chem. 259: 5197–5207.

Tamura, K. and Hasegawa, T. (1997). Role of the CCA end of tRNA and its vicinity in aminoacylation. Nucleic Acids Symp. Ser. 37: 133–134.

Tanaka, N., Chakravarty, A.K., Maughan, B., and Shuman, S. (2011). Novel mechanism of RNA repair by RtcB via sequential 2′, 3′-cyclic phosphodiesterase and 3′-phosphate/5′-hydroxyl ligation reactions. J. Biol. Chem. 286: 43134–43143.

Tavtigian, S.V., Simard, J., Teng, D.H., Abtin, V., Baumgard, M., Beck, A., Camp, N.J., Carillo, A.R., Chen, Y., Dayananth, P., et al. (2001). A candidate prostate cancer susceptibility gene at chromosome 17p. Nat. Genet. 27: 172–180.

Thompson, D.M. and Parker, R. (2009). Stressing out over tRNA cleavage. Cell 138: 215–219.

Tomita, K. and Yamashita, S. (2014). Molecular mechanisms of template-independent RNA polymerization by tRNA nucleotidyltransferases. Front. Genet. 5: 36.

Trotta, C.R., Paushkin, S.V., Patel, M., Li, H., and Peltz, S.W. (2006). Cleavage of pre-tRNAs by the splicing endonuclease requires a composite active site. Nature 441: 375–377.

Tsuboi, T., Yamazaki, R., Nobuta, R., Ikeuchi, K., Makino, S., Ohtaki, A., Suzuki, Y., Yoshihisa, T., Trotta, C., and Inada, T. (2015). The tRNA splicing endonuclease complex cleaves the mitochondria-localized CBP1 mRNA. J. Biol. Chem. 290: 16021–16030.

Vogel, U.S. and Thompson, R.J. (1987). Molecular cloning of the myelin specific enzyme 2′, 3′-cyclic-nucleotide 3′-phosphohydrolase. FEBS Lett. 218: 261–265.

Weinger, J.S., Parnell, K.M., Dorner, S., Green, R., and Strobel, S.A. (2004). Substrate-assisted catalysis of peptide bond formation by the ribosome. Nat. Struct. Mol. Biol. 11: 1101–1106.

Weitzer, S. and Martinez, J. (2007). The human RNA kinase hClp1 is active on 3′ transfer RNA exons and short interfering RNAs. Nature 447: 222–226.

Wellner, K., Betat, H., and Morl, M. (2018a). A tRNA's fate is decided at its 3′ end: collaborative actions of CCA-adding enzyme and RNases involved in tRNA processing and degradation. Biochim. Biophys. Acta Gene Regul. Mech. 1861: 433–441.

Wellner, K., Czech, A., Ignatova, Z., Betat, H., and Morl, M. (2018b). Examining tRNA 3′-ends in *Escherichia coli*: teamwork between CCA-adding enzyme, RNase T, and RNase R. RNA 24: 361–370.

Wilusz, J.E., Whipple, J.M., Phizicky, E.M., and Sharp, P.A. (2011). tRNAs marked with CCACCA are targeted for degradation. Science 334: 817–821.

Wu, J., Bao, A., Chatterjee, K., Wan, Y., and Hopper, A.K. (2015). Genome-wide screen uncovers novel pathways for tRNA processing and nuclear-cytoplasmic dynamics. Genes Dev. 29: 2633–2644.

Wu, J., Niu, S., Tan, M., Huang, C., Li, M., Song, Y., Wang, Q., Chen, J., Shi, S., Lan, P., et al. (2018). Cryo-EM structure of the human ribonuclease P holoenzyme. Cell 175: 1393–1404.e11.

Xue, S., Calvin, K., and Li, H. (2006). RNA recognition and cleavage by a splicing endonuclease. Science 312: 906–910.

Yamashita, S., Takeshita, D., and Tomita, K. (2014). Translocation and rotation of tRNA during template-independent RNA polymerization by tRNA nucleotidyltransferase. Structure 22: 315–325.

Yamashita, S. and Tomita, K. (2016). Mechanism of 3′-matured tRNA discrimination from 3′-immature tRNA by class-II CCA-adding enzyme. Structure 24: 918–925.

Yoshihisa, T. (2014). Handling tRNA introns, archaeal way and eukaryotic way. Front. Genet. 5: 213.

Zhang, J. and Ferre-D'amare, A.R. (2016). The tRNA elbow in structure, recognition and evolution. Life (Basel) 6, https://doi.org/10.3390/life6010003.

Zuko, A., Mallik, M., Thompson, R., Spaulding, E.L., Wienand, A.R., Been, M., Tadenev, A.L.D., Van Bakel, N., Sijlmans, C., Santos, L.A., et al. (2021). tRNA overexpression rescues peripheral neuropathy caused by mutations in tRNA synthetase. Science 373: 1161–1166.